Supplementary Information

Bimetallic Mo-Co Nanoparticles Anchored on Nitrogen-Doped Carbon for Enhanced Electrochemical Nitrogen Fixation

Yizhen Zhang,[1,4] Jue Hu,[2,*] Chengxu Zhang,[3,*] Yizhe Liu,[1] Mengyuan Xu,[2] Yujia Xue,[1] Lifen Liu,[4] Michael K. H. Leung,[1,*]

[1]Ability R&D Energy Research Centre, School of Energy and Environment, City University of Hong Kong, Hong Kong, China

[2]Faculty of Science, Kunming University of Science and Technology, Kunming, China

[3]The Engineering Laboratory of Advanced Battery and Materials of Yunnan Province, Faculty of Metallurgical and Energy Engineering, Kunming University of Science and Technology, Kunming, China

[4]Key Laboratory of Industrial Ecology and Environmental Engineering (MOE), School of Environmental Science and Technology, Dalian University of Technology, Dalian, China

*Corresponding author.

E-mail addresses: hujue@kust.edu.cn (J. Hu), chxzhang@kust.edu.cn (C. Zhang), mkh.leung@cityu.edu.hk (M. Leung)

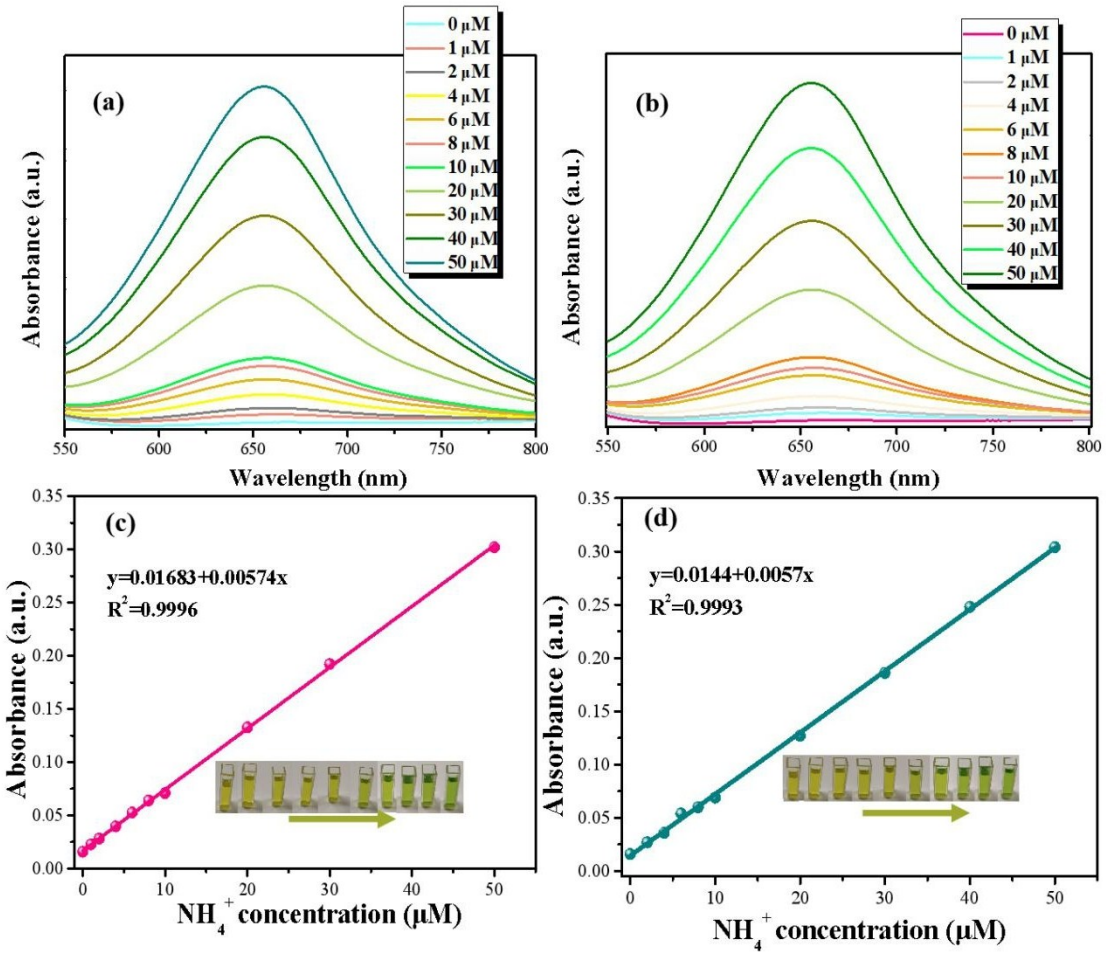

Fig. S1 UV-vis curves of indophenol assays after being incubated for 2 h in (a) 0.1 M Na_2SO_4 and (b) 0.1 mM H_2SO_4; calibration curves used for estimation of NH_3 concentration in (c) 0.1 M Na_2SO_4 and (d) 0.1 mM H_2SO_4 (Insert picture is the chromogenic reaction solution with indophenol indicator of increased NH_4^+ concentration) [11]

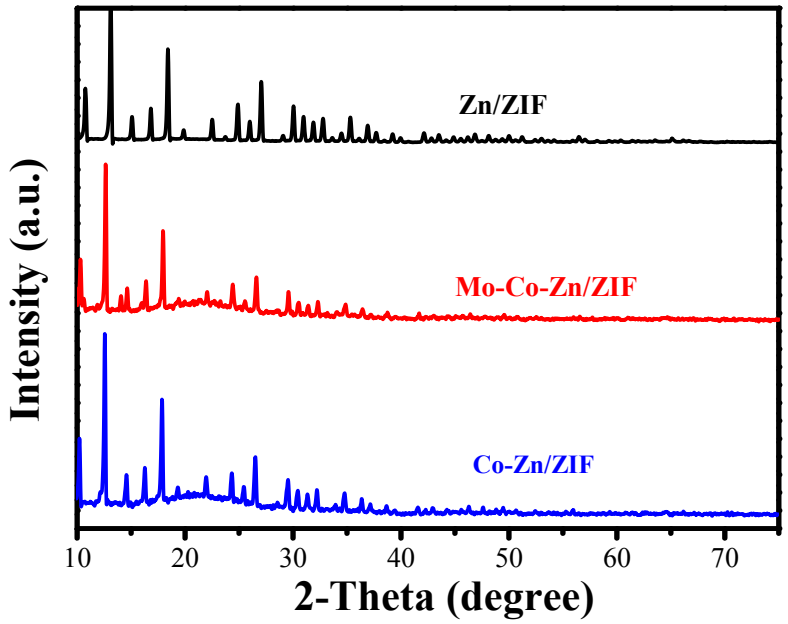

Fig. S2 XRD patterns of pristine Zn-ZIFs, Co-Zn/ZIFs and Mo-Co-Zn/ZIFs.

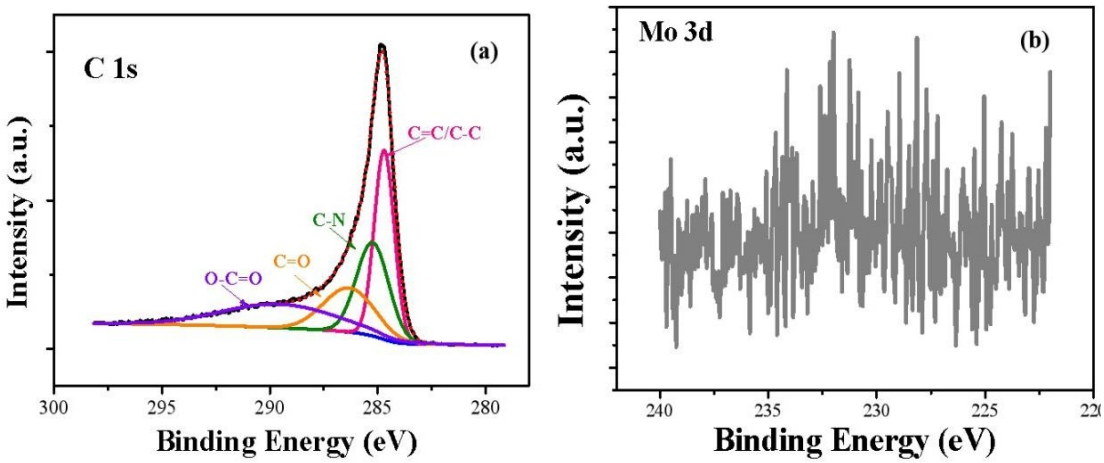

Fig. S3 XPS spectrum for (a) C 1s and (b) Mo 3d of Co/NC.

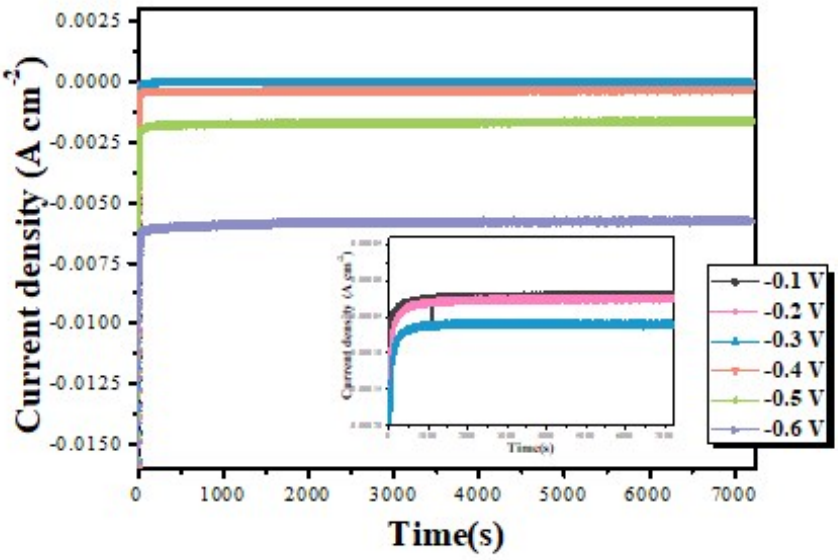

Fig. S4 Chrono-amperometry results of Co/NC at different applied potentials.

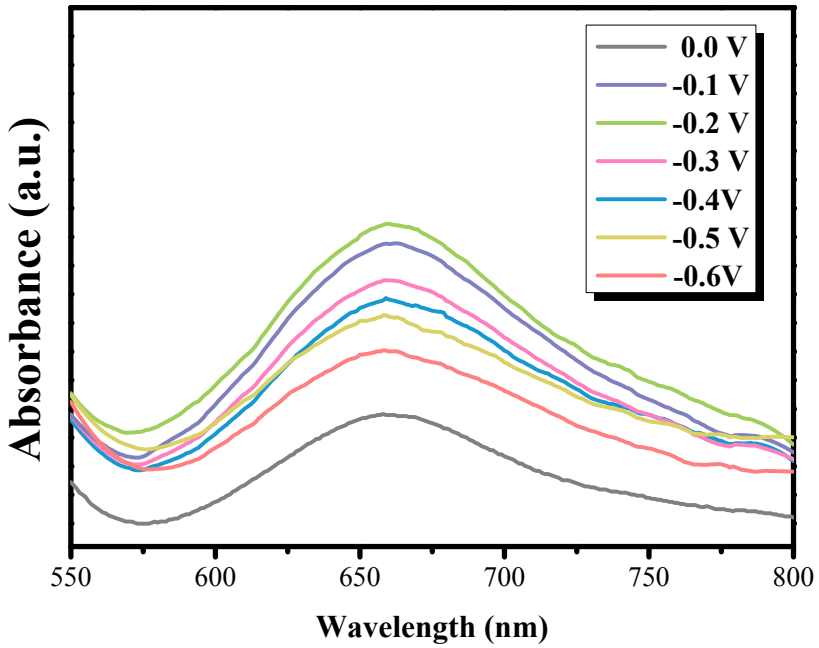

Fig. S5 UV−Vis absorbance of Co/NC in N_2-saturated 0.1 M Na_2SO_4 electrolyte for 2 h electrolysis at the corresponding applied potentials.

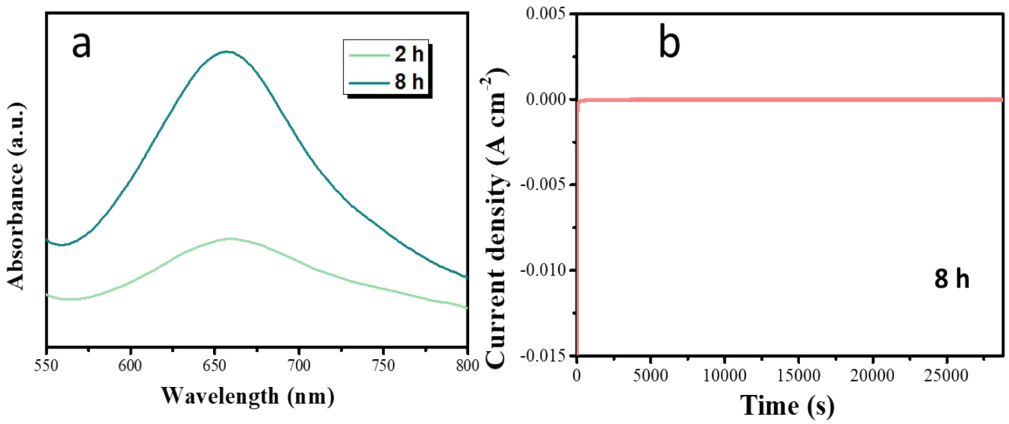

Fig. S6 (a) Comparison UV-Vis absorption spectra of the electrolytes for Mo-Co/NC after electrolysis at -0.1 V (vs. RHE) in N_2 for 2h and 8h and (b) chronoamperometry results of 8h electrolysis at -0.1 V (vs. RHE).

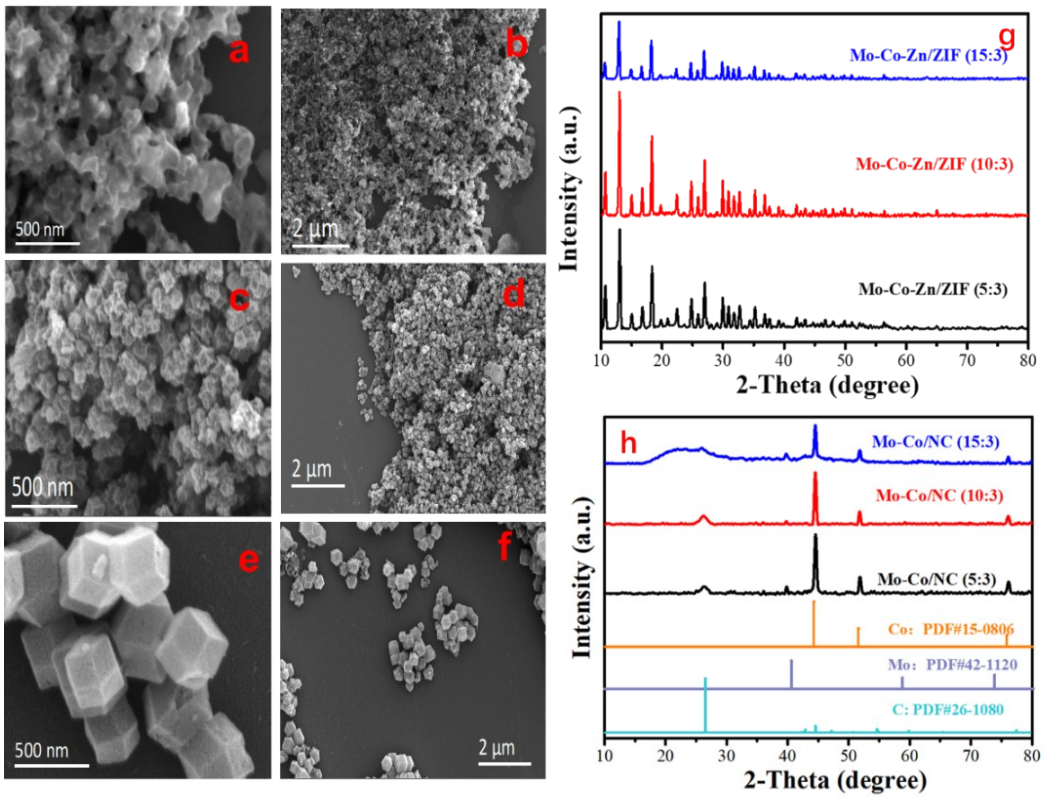

Fig. S7 SEM images of (a, b) Mo-Co/NC (5:3), (c, d) Mo-Co /NC (10:3) and (e, f) Mo-Co/NC (15:3), XRD patterns of catalysts before and after pyrolysis.

The morphology and structure of Mo-Co/NC (15:3), Mo-Co /NC (10:3) and Mo-Co/NC (5:3) were compared with Mo-Co/NC. Comparisons of the XRD patterns before and after pyrolysis were displayed in Fig. S7. ZIF precursors before pyrolysis agreed well with the experimental sample in the literatures reported previously. In comparison to the Mo-Co/NC with broad carbon peaks (Fig. 1j), a series of Mo-Co /NC (15:3, 10:3, 5:3) exhibit obvious Co peaks (PDF#15-0806) and Mo peak (PDF#42-1102), as well as relative weak carbon peaks, indicating the presence of metallic aggregates[2]. As displayed by the SEM images (Fig. S7), Mo-Co/NC (15:3) and Mo-Co /NC (10:3) showed similar features in morphology and structure as Mo-Co/NC dodecagon shape. Mo-Co/NC (10:3) preserved the morphology with smaller size and slight surface contraction. However, with the decrease of the Zn^{2+} concentration, the morphology of Mo-Co/NC (5:3) was changed and particles were aggregated together, revealing that zinc could act as a spacer to prevent aggregation of metals and tuning the zinc dopant content could help in obtaining the carbon structure[3].

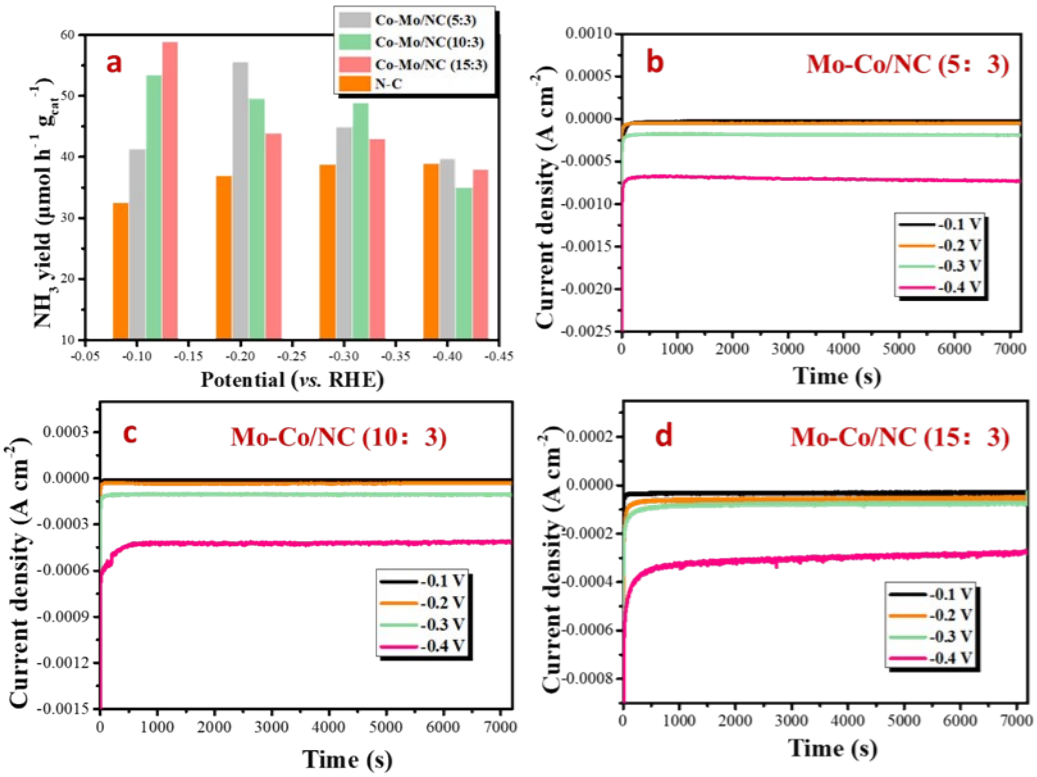

Fig. S8 (a) NH_3 yield rate and (b) corresponding chronoamperometry results at different applied potentials in N_2-saturated electrolyte.

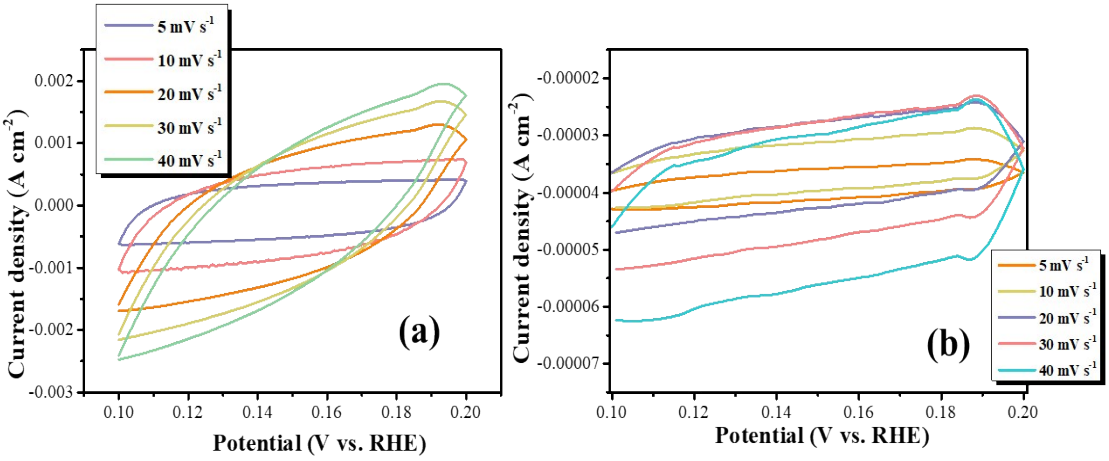

Fig. S9 Double-layer capacitance measurement for determining electrochemically active surface area (EASA). CV of carbon paper working electrode with (a) Co/NC, (b) without any catalyst at various scan rates (5 to 40 mV s^{-1}) in the non-faradaic region of 0.1 to 0.2 V vs. RHE.

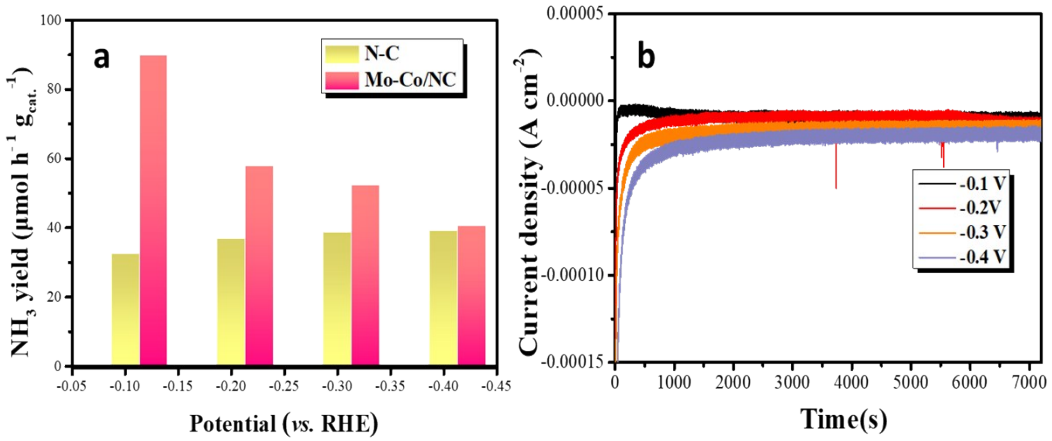

Fig. S10 (a) NH_3 yield of Mo-Co/NC (red) and N-C (red) at different applied potentials in N_2-saturated electrolyte, (b) chronoamperometry results of N-C at different applied potentials.

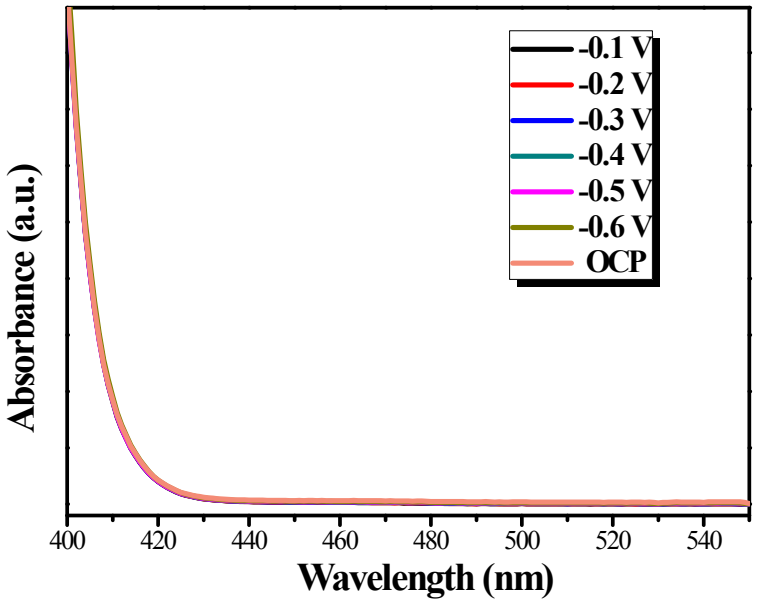

Fig. S11 UV-Vis absorption spectra of the detected electrolyte with Mo-Co/NC catalyst stained with the indicator for $N_2H_4 \cdot H_2O$[4].

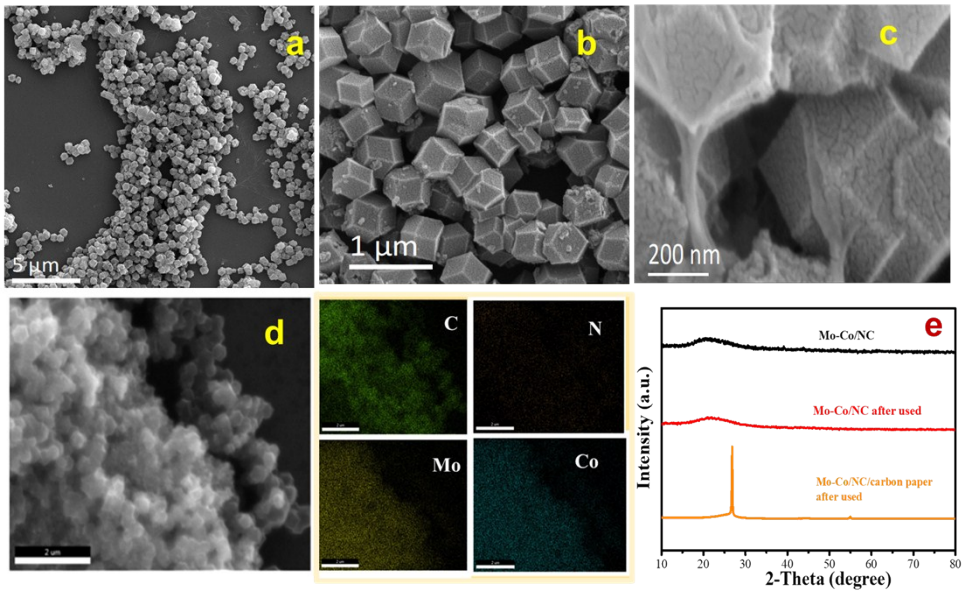

Fig. S12 (a, b, c) SEM images of Mo-Co/NC after electrolysis, (d) corresponding EDS-mapping in selected area, and (e) XRD patterns of Mo-Co/NC before and after electrolysis in powder and on carbon paper.

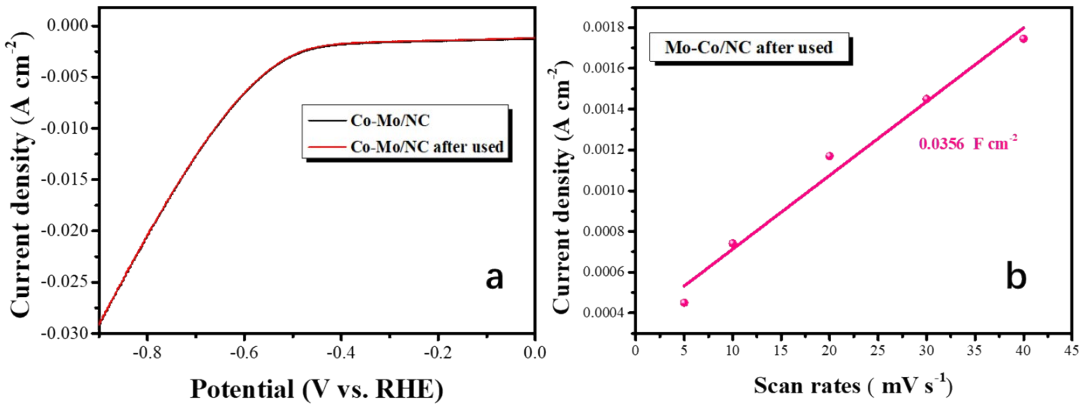

Fig. S13 (a) Linear sweep voltammetry (LSV) curves of Mo-Co/NC before and after used in N_2-saturated 0.1 M aqueous Na_2SO_4 at a scan rate of 10 mV s^{-1}, (b) charging current density differences plotted against scan rates for carbon paper working electrode with Mo-Co/NC.

The characterizations were explored by electrochemical test, SEM, EDS-mapping, and XRD, to confirm the stability of catalyst. As displayed in Fig. S12, the Mo-Co/NC after electrolysis still maintain the original morphology and structure, and was connected together with Nafion solution (Fig. S12 c). EDS-mapping images revealed that the C, N, Mo, Co are uniform distribution (Fig. S12 d). Additionally, the structure and chemical composition of Mo-Co/NC after electrolysis were compared by XRD, without any changes (Fig. S12 e). Furthermore, the comparison of LSV and ECSA tests was also performed, indicating the electrochemical stability of Mo-Co/NC (Fig. S13).

Table S1 ICP-AES results of prepared catalysts

Sample	Co content (wt%)	Mo content (wt%)
N-C	0	0
Mo-Co/NC (5:3)	18.22	4.67
Mo-Co/NC (10:3)	16.38	3.68
Mo-Co/NC (15:3)	9.83	2.12
Mo-Co/NC	1.15	1.38

Table S2. Summary of the NRR performances for some reported electrocatalysts

Material	Electrolyte	Yield	FE (%)	Potential	Ref.
N-doped porous carbon	0.05 M H_2SO_4	1.40 mmol g^{-1} h^{-1}	1.42	–0.9 V vs. RHE	ACS Catal., 8 (2018), 1186
$Pd_{0.2}Cu_{0.8}$/rGO	0.1 M KOH	2.8 μg h^{-1} $mg_{cat.}^{-1}$	~4.5	–0.2 V vs. RHE	Adv. Energy Mater., 8 (2018) , 1800124
(110)-oriented Mo	Aqueous solutions	3.09×10^{-11} mol s^{-1} cm^{-2}	0.7	–0.49 V vs. RHE	J. Mater. Chem. A, 5 (2017), 18967-18971
Au film	0.1 M KOH	3.84×10^{-12} mol cm^{-2} s^{-1}	<1	–0.5 V vs. RHE	J. Am. Chem. Soc., 140 (2018), 1496
N,P -doped porous carbon (NPC)	0.1 M HCl	0.97 μg h^{-1} $mg_{cat.}^{-1}$	4.2	-0.2 V vs. RHE	Chem. Commun., 55 (2019), 687-690
Cobalt/Nitrogen -Doped Carbon	0.1 M KOH	5.1 μg h^{-1} $mg_{cat.}^{-1}$	10.1	-0.4 V vs. RHE	ACS Appl. Energy Mater., 2 (2019), 6071-6077
PdZn	0.1 M PBS	5.28 μg mg^{-1} $_{cat.}$ h^{-1}	16.9	-0.2 V vs. RHE	Appl. Catal. B Environ., 265 (2020), 118568
Mo_2C/C	0.5 M Li_2SO_4	11.3 μg h^{-1} mg^{-1}_{Mo2C}	7.8	-0.3 V vs. RHE	Adv. Mater., 30 (2018), 1803694
Mo_3Fe_3C	0.1 M Li_2SO_4	72.5 μmol h^{-1} $g_{cat.}^{-1}$	27	-0.05 V vs RHE	Nano Energy, 68 (2020), 104374
Mo-Co/NC	**0.1 M Na_2SO_4**	**89.8 μmol h^{-1} $g_{cat.}^{-1}$**	**13.5**	**-0.1 vs RHE**	**This work**

Table S3 Summary of crystalline sizes calculated by Scherrer's equation

Planes	Mo-Co/NC (5:3)	Mo-Co/NC (10:3)	Mo-Co/NC (15:3)
(111)	25.494	26.697	23.132
(200)	27.041	20.265	18.665
(220)	34.895	23.265	22.182
Average	29.143	23.595	21.3265

References:

1. D. Zhu, L. Zhang, R. E. Ruther and R. J. Hamers, *Nat. Mater.*, 2013, **12**, 836-841.
2. S. Mukherjee, X. Yang, W. Shan, W. Samarakoon, S. Karakalos, D. A. Cullen, K. More, M. Wang, Z. Feng, G. Wang and G. Wu, *Small Methods*, 2020, 1900821.
3. L. Han, X. Liu, J. Chen, R. Lin, H. Liu, F. Lü, S. Bak, Z. Liang, S. Zhao, E. Stavitski, J. Luo, R. R. Adzic and H. L. Xin, *Angew. Chem. Int. Ed.*, 2019, **58**, 2321-2325.
4. J. D. C. George W. Watt, *Anal. Chem.*, 1952, 24, 12, 2006-2008.